International Journal of Nanomedicine

Dovepress
open access to scientific and medical research

Open Access Full Text Article

ORIGINAL RESEARCH

EGFR-Targeted and NIR-Triggered Lipid-Polymer Hybrid Nanoparticles for Chemo-Photothermal Colorectal Tumor Therapy

Fang Fang[1,*], Yun Yan Chen[1,*], Xin-Ming Zhang[2], Jin Tang[1], Yu-Hao Liu[1], Chen-Shuo Peng[1], Yu Sun[1,3]

[1]School of Pharmacy, Wannan Medical College, Wuhu, 241002, People's Republic of China; [2]School of Chemistry and Materials Science, Anhui Normal University, Wuhu, 241002, People's Republic of China; [3]Institute of Synthesis and Application of Medical Materials, Wannan Medical College, Wuhu, 241002, People's Republic of China

*These authors contributed equally to this work

Correspondence: Yu Sun, School of Pharmacy, Wannan Medical College, Wuhu, 241002, People's Republic of China, Tel +86 553 3932026, Email whsunyu@163.com

Background: Epidermal growth factor receptor (EGFR) is a major target for the treatment of colorectal cancer. Thus, anti-EGFR antibody conjugated lipid-polymer hybrid nanoparticles can offer a potential means of enhancing the efficacy of chemotherapeutics in EGFR overexpressing cancers. In addition, the combination of chemotherapy and photothermal therapy is a promising strategy for cancer treatment. Hence, it is highly desirable to develop a safe and effective delivery system for colorectal tumor therapy.

Methods: In this study, EGFR-targeted and NIR-triggered lipid-polymer hybrid nanoparticles (abbreviated as Cet-Iri-NPs) were prepared with copolymer PPG-PEG, lipids DSPE-PEG-Mal and lecithin as carriers, CPT-11 as an anticancer chemotherapeutic agent, indocyanine green (ICG) as a photothermal agent, and cetuximab as a surface-targeting ligand.

Results: In vitro analyses revealed that Cet-Iri-NPs were spherical with size of 99.88 nm, charge of 29.17 mV, drug entrapment efficiency of 51.72%, and antibody conjugation efficiency of 41.70%. Meanwhile, Cet-Iri-NPs exhibited a remarkable photothermal effect, and pH/NIR-triggered faster release of CPT-11 with near infrared (NIR) laser irradiation, which induced enhanced cytotoxicity against SW480 cells. Furthermore, the promoted tumor-growth suppression effect of Cet-Iri-NPs on SW480 tumor xenograft nude mice was achieved under NIR laser irradiation.

Conclusion: These results indicate that the well-defined Cet-Iri-NPs are a promising platform for targeted colorectal cancer treatment with chemo-photothermal therapy.

Keywords: Chemo-photothermal therapy, Targeted cancer therapy, Nanoparticles, Cetuximab, Indocyanine green

Background

Colorectal cancer (CRC) ranks third among the most common malignancies globally.[1,2] Furthermore, metastatic CRC is considered one of the most uncurable cancers. Approximately 70% to 75% of patients diagnosed with metastatic CRC survive beyond 1 year, 30% to 35% beyond 3 years, and less than 20% beyond 5 years from diagnosis.[3] Nowadays, combination therapy is recommended as the primary treatment for unresectable metastatic CRC. Chemotherapy, particularly Irinotecan (CPT-11, IRT), remains the first-line treatment for metastatic colorectal cancer after failure of standard chemotherapy regimens. Nevertheless, several significant side effects such as severe delayed diarrhea, neutropenia, and liver damage restrict the IRT use.[4] These various toxicities can result in treatment interruption or cessation, thereby jeopardizing the prognosis and quality of life of the patients, even those patients in relatively good condition. Consequently, there is a need to find new therapeutic strategies to improve clinical therapeutic effects and patient compliance with traditional chemotherapy.

Received: 12 April 2024
Accepted: 30 August 2024
Published: 18 September 2024

Graphical Abstract

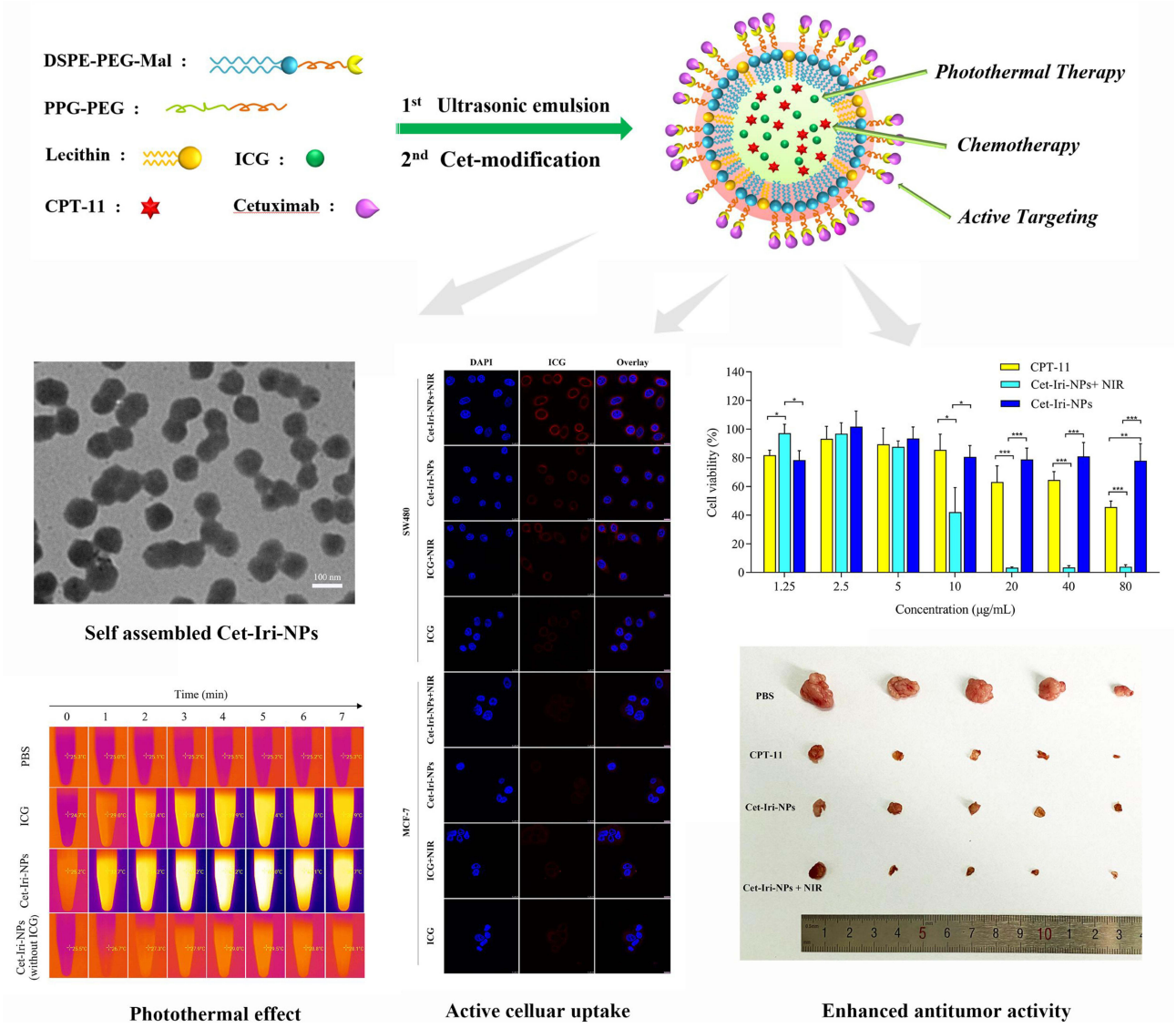

Photothermal therapy (PTT) is a cancer therapeutic strategy with high specificity, nontoxicity and controllability, which destroys the bioactive molecules in cells, resulting in tumor cell damage, necrosis or thermal ablation of tumor tissue.[5,6] However, PTT effectiveness is limited by the photothermal conversion efficiency of photothermal agents. To overcome the shortcomings of monotherapy, the synchronous application of chemotherapy and photothermal therapy (chemo-photothermal therapy) has become a research hotspot.[7–9] With the irradiation of loaded near-infrared (NIR) sensitive photosensitizers, chemo-photothermal therapy can significantly improve the therapeutic effect, leading to low doses of chemotherapy drugs, reduced side effects and metastasis, and even complete eradication of tumor.[10–12] Indocyanine green (ICG), an amphiphilic fluorescent dye approved by the US Food and Drug Administration (FDA) in 1959, has been used extensively in optically mediated diagnostic and therapeutic applications. In view of its distinctive features of converting NIR light to heat and generating reactive oxygen species (ROS) in the presence of NIR light, ICG can been used for photothermal therapy (PTT) and photodynamic therapy (PDT).[13–15] Moreover, ICG is encapsulated in co-delivery nanoplatforms to overcome its drawbacks, such as instability, short plasma half-life, lack of targeting ability,

and self-aggregation under physiological conditions.[13,16] Hence, ICG is considered to be a promising photosensitizer for chemo-photothermal therapy.[17,18]

To achieve chemo-photothermal therapy at full capacity, multifunctional nanoparticles (NPs) have also been applied as platforms for chemotherapeutic drugs.[19–21] For the surface modification method, polyethylene glycol conjugation (PEGylation) is always considered as the best approach for nanoparticles to avoid the recognition and clearance of reticuloendothelial system (RES), thus prolonging the circulation time in the blood.[22–25] However, exploitation of this method alone is often inadequate. Biological ligands, including antibodies, peptides, and polysaccharides, are often bound to the surface of NPs to achieve active targeting, which could increase the cellular uptake of drug-loaded NPs and improve their therapeutic efficacy.[26–28] Thus, PEGylated and antibody-conjugated multifunctional NPs may be a promising therapeutic strategy to improve the therapeutic effects of chemo-photothermal drug delivery nano-systems. Cetuximab, an IgG1 monoclonal antibody against Epidermal growth factor receptor (EGFR) approved by the FDA in February 2004, is mainly used for the treatment of metastatic CRC, locally advanced or recurrent/metastatic head and other malignant solid tumors[29]. In the treatment of KRAS wild-type metastatic CRC, the combination of cetuximab and irinotecan is relatively common and has an outstanding therapeutic effect[30,31]. In addition, cetuximab can specifically recognize and bind to the highly expressed EGFR antigen on the surface of tumor cells. In recent years, it has gradually been used as an active targeting factor to develop agents with active targeting ability.[32,33] Our previous studies have indicated that cetuximab-modified indocyanine green (ICG) and anticancer drug-co-loaded nanoparticles can produce hyperthermia and ROS under NIR irradiation, thereby enhance therapeutic efficacy.[34,35]

Recent studies have shown that PEGylated poly(N-phenylglycine) (PPG-PEG) has advantages in anchoring ICG via π-π stacking interactions to avoid premature leakage and to convert low-dose NIR light to induce localized hyperthermia to enhance the photothermal effect.[16,36] To the best of our knowledge, this copolymer has not been previously used in active targeted drug delivery systems. This study aims to address these challenges by developing a novel active targeted drug delivery system. By using ICG as a photothermal agent and cetuximab as a surface-targeting ligand, lipid-polymer hybrid nanoparticles (denoted as Cet-Iri-NPs) could enhance the selectivity of irinotecan delivery to EGFR-overexpressing SW480 cells and achieve chemo-photothermal therapy.

Materials and Methods

Materials

Cetuximab was purchased from Meilunbio (Dalian, China). Egg yolk lecithin, methoxy poly(ethylene glycol) amine (mPEG-NH_2) (MW 5000), and 1.2-distearoyl-sn-glycero-3-phosphoethanolamine-N-[maleimide(polyethylene glycol) 2000] (DSPE-PEG_{2000}-Mal) with the purity above 99.0% were purchased from Ponsure Biological Co., Ltd. (Shanghai, China). Irinotecan hydrochloride, indocyanine green, N-phenylglycine (PG), and other obtained from Innochem Science and Technology Co., Ltd. (Beijing, China). Enhanced Cell Counting Kit-8 (CCK-8), BCA protein assay kit, and DAPI staining solution were purchased from Beyotime Biotechnology Co. Ltd. (Nanjing, China).

Synthesis of the PEGylated Copolymer

As shown in Figure 1, the polymer poly(N-phenylglycine) (PPG) was synthesized according to a previous reported method.[36] Then, the PEGylated copolymer PPG-PEG was synthesized by an acylation reaction between the carboxyl side-chains of PPG and amino end-groups of mPEG-NH_2. Briefly, 0.03 g PPG (0.2 mmol of PG unit) was dissolved in 15 mL DMSO, and then 0.15 g (1.5 mmol) EDC and 0.12 g (1 mmol) NHS were added and stirred at room temperature for 2 h to activate the carboxyl group. Subsequently, 0.5 g (0.1 mmol) mPEG-NH_2 was added to the reaction mixture and degassed under nitrogen atmosphere. The resultant mixture was then reacted at 50°C in the dark for 72 h. Then, the reaction mixture was packed into dialysis bags and dialyzed in ultrapure water for 7 days. Finally, the product PPG-PEG was obtained as a dark blue powder by lyophilization. Yield: 216 mg (83.1%).

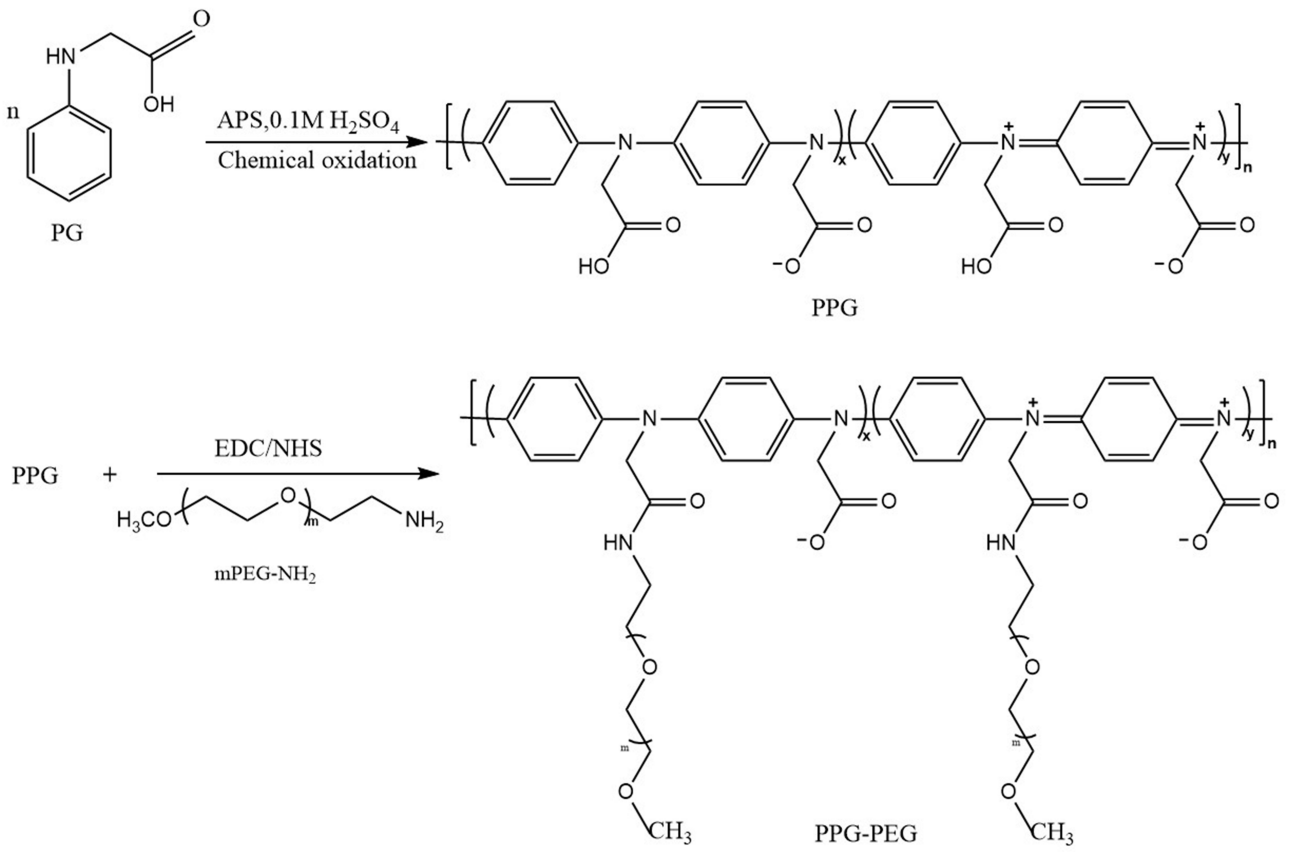

Figure 1 Synthetic route of PPG-PEG.

Preparation of PPG-Based Targeted Drug-Loaded Nanoparticles

PPG-based targeted drug-loaded nanoparticles (Cet-Iri-NPs) were fabricated using a facile ultrasonic self-assembly method, as described in our previous work.[34,35,37] First, lipid-polymer hybrid drug-loaded nanoparticles (denoted as Iri-NPs) were prepared from PPG-PEG, lecithin, DSPE-PEG-Mal, CPT-11, and ICG using a single-step ultrasonic emulsion method. Stock solutions for the preparation of Iri-NPs were PPG-PEG: 2.0 mg/mL in acetonitrile solution; lecithin and DSPE-PEG-Mal: 1 mg/mL in 4 wt% ethanol aqueous solution, respectively; CPT-11 and ICG: 1 mg/mL in ultrapure water, respectively. First, 0.5 mL lecithin, 0.5 mL DSPE-PEG-Mal, 1 mL CPT-11, and 1 mL ICG solution were dispersed in 8 mL water. Subsequently, 1 mL PPG-PEG solution was added dropwise to the above suspension under sonication (20 kHz, 285 W). After ultrasonic emulsified for another 12 min, the resulting emulsion Iri-NPs were filtered and concentrated with an amicon ultra-15 centrifugal filter (10 kDa) for further use. To obtain targeted nanoparticles (Cet-Iri-NPs), cetuximab was first thiolated by Traut's reagent and then reacted with Iri-NPs with a molar ratio of 1:100 in phosphate buffer saline (PBS, pH 8.5–9.0) solution at 4°C for 24 h. The unreacted maleimide groups on the surface of the nanoparticles were blocked off with 0.5 μL 2-mercaptoethanol. Finally, pure Cet-Iri-NPs were isolated and concentrated by above ultracentrifuge method. The same procedure was used to prepare Cet-Iri-NPs without ICG in the absence of ICG.

Characterization of PPG-Based Targeted Drug-Loaded Nanoparticles

The morphology of Cet-Iri-NPs was observed by TEM (JEM-100XII, Tokyo, Japan) with negative stain method. Before analysis, the samples were stained with 2% (w/v) phosphotungstic acid, and then placed on a copper grid with films and dried at room temperature overnight prior to imaging. Hydrodynamic diameter and PDI were determined using dynamic light scattering (DLS) (NANO ZS92, Malvern, UK) at room temperature. The encapsulation efficiency (EE) and loading efficiency (LE) of CPT-11 and ICG encapsulated in Cet-Iri-NPs

were determined using a UV/Vis spectrophotometer as follows: Some freeze-dried Cet-Iri-NPs were accurately weighed and thoroughly dissolved in DMSO under ultrasonication to obtain a homogeneous solution. The absorbance of CPT-11 and ICG in the above solution was measured using a UV/Vis spectrophotometer at 370 and 779 nm, respectively. The EE and LE were calculated using the following equations:

$$\mathrm{EE}(\%) = \frac{\text{Weight of loaded drug}}{\text{Weight of initially added drug}} \times 100$$

$$\mathrm{LE}(\%) = \frac{\text{Weight of loaded drug}}{\text{Weight of nanoparticles}} \times 100$$

The protein concentration of Cetuximab in Cet-Iri-NPs was determined by the bicinchoninic acid (BCA) method.[35,38] The concentrations of Cetuximab (2–10 μg) in 200 μL BCA reagent were used for the standard curve. Nanoparticles without cetuximab modification were chosen as controls.

Study of Photothermal Conversion Performance

To evaluate the photothermal properties of Cet-Iri-NPs mediated by ICG, 1 mL of aqueous Cet-Iri-NPs solution (containing 80 μg/mL ICG) was placed in a 1.5 mL centrifuge tube. Equal volumes of PBS buffer solution, free ICG (80 μg/mL), and Cet-Iri-NPs (absence of ICG) aqueous solution were chosen as controls. All samples were irradiated by an NIR laser (808 nm, 1.6 W/cm^2) for 5 min, and real-time temperatures were recorded by the infrared thermal imaging camera (XthermT3, China).

NIR/pH-Triggered in vitro Drug Release

In vitro drug release experiment was performed using a dialysis method. 1mL Cet-Iri-NPs solution was sealed into dialysis bags (MWCO 3000) in quadruplicate. For NIR activation, samples were irradiated for 5 min using a near-infrared laser (808 nm, 1.6 W/cm^2) and then respectively dialyzed against 50 mL of PBS (pH 7.4) and PBS (pH 5.0) under gentle stirring at 37°C. The remaining samples were directly dialyzed against 50 mL of PBS (pH 7.4) and PBS (pH 5.0) according to the similar procedure except NIR irradiation. At predetermined time intervals, 1.5 mL of release medium was withdrawn and replaced with an equal volume of fresh PBS for further study. The amount of CPT-11 released from the Cet-Iri-NPs was quantified by UV-vis spectrophotometry. Cumulative drug release (R_n) was calculated using Equations (3).

$$Er(\%) = \frac{V_e \sum_1^{n-1} C_i + V_0 C_n}{M} \times 100$$

Where M is the total mass of CPT-11 in the Cet-Iri-NPs, V_0 is the total volume of the release buffer (V_0 = 50 mL), C_n is the concentration of CPT-11 in the nth sample.

Cell Culture

The human colorectal cancer cell line SW480 and human breast cancer cell line MCF-7 were purchased from the Shanghai Institute of Cell Biology, Chinese Academy of Sciences. Cells were cultured in DMEM (Gibco) supplemented with 10% fetal bovine, 1% penicillin, and streptomycin under a humidified 5% CO_2 atmosphere at 37°C. The cells were trypsinized, passaged every 2–3 days and collected in the logarithmic growth phase.

In vitro Cellular Uptake Study

Confocal laser scanning microscopy (CLSM) (Leica SP8, GER) was used to observe the in vitro intracellular distribution and internalization of Cet-Iri-NPs. Briefly, SW480 and MCF-7 cells (5 × 10^4 cells/dish) were seeded in confocal dishes (φ 2cm) respectively and cultured overnight. Then, the medium was replaced with fresh culture medium containing Cet-Iri-NPs (containing 20 μg/mL CPT-11) or free ICG (containing the same ICG in Cet-Iri-NPs). Cells in the experimental groups were exposed to an NIR laser (1.6 W/cm^{2,} 808 nm) for 5 min.

After incubation for 3 h, the cells were washed twice with PBS to remove unbound NPs and fixed with 4% paraformaldehyde solution for 15 min. Finally, the nuclei were stained with 800 uL DAPI for 5 min and washed with PBS for 3 times. Subsequently, the cells were observed by a confocal laser scanning microscope (CLSM). In fluorescence imaging, the nucleoli were located at λ_{EX} 405 nm, and ICG at λ_{EX} 561 nm.

Intracellular ROS Detection

Intracellular reactive oxygen species (ROS) generation was measured using the DCFH-DA ROS Assay kit.[39,40] Briefly, SW480 cells were seeded in a confocal dish at a density of 1×10^5 cells/dish. After incubated with 2 mL DMEM for 24 h, the original medium was removed, and the cells were washed twice with PBS. To investigate the ROS generation efficiency of ICG, the cells were incubated with free CPT-11 (10 μg/mL), free ICG (12 μg/mL), and Cet-Iri-NPs (containing 10 μg/mL CPT-11 and 12 μg/mL ICG). Cells incubated without drugs were used as controls. DCFH-DA (Biosharp, China), a ROS-sensitive probe, was used to detect intracellular ROS generation. After 0.5 h incubation, the cells were exposed to NIR irradiation (808 nm, 1.6 W/cm^2) for 5 min. After 6 h incubation, the cells were washed with PBS, and fresh culture medium containing DCFH-DA (20 mM) was added for an additional 20 min incubation in the dark. Then the medium was replaced with PBS and fluorescence images of the treated cells were acquired using CLSM.

Cell Cytotoxicity Assay

For cytotoxicity evaluation, the CCK8 assay was performed using SW480 cells.[41] Briefly, SW480 cells (5×10^3 cells/well) were seeded in 96-well plates and cultured in 100 μL DMEM for 24 h. Then, various concentrations (ranging from 1.25 to 80 μg/mL) of free CPT-11 or Cet-Iri-NPs (containing same concentration of CPT-11) were added to the culture wells. To explore the effect of photothermal therapy, cells treated with Cet-Iri-NPs were irradiated with a 1.6 W/cm^2 808 nm laser for 3 min. While for chemotherapy alone, the cells were not exposed to the NIR laser. After incubation for another 24 h, 10 μL enhanced cell counting kit (CCK8) solution was immediately added to each well and mixed gently. After incubation for another 2 h, the absorbance of each well was measured at 450 nm using a microplate reader (Thermo Fisher Scientific). The cell viability of each group was calculated using Equations (4).

$$\text{Cell viability}(\%) = \frac{A_{test} - A_{blank}}{A_{control} - A_{blank}} \times 100$$

Cell Apoptosis Assay

The cell apoptosis assay was assessed by using the Annexin V-FITC Apoptosis Detection Kit. Briefly, SW480 cells were seeded in 6-well plates (2×10^5 cells/well) and incubated for 24 h. The cells were cultured in medium containing free CPT-11, ICG, or Cet-Iri-NPs (containing the same concentration of drug and ICG) and subsequently irradiated with an NIR laser (808 nm, 1.6 W/cm^2) for 5 min. While for chemotherapy alone, cells were not exposed to 808nm laser. After cultured for another 24 h, the cells were collected and labeled with 5 μL Annexin V-FITC and 10 μL propidium iodide. After that, flow cytometry (FACSVerse, BD, USA) was used to detect cell apoptosis.

Animal Model

All animal experiments were performed in accordance with the Guide for the Care and Use of Laboratory Animals (US National Research Council, 2011), and approved by the Committee for Experimental Animal Welfare and Ethics of Wannan Medical College (No. LLSC-2022-045). Nude mice (BALB/c, 25 ± 2 g) were acquired from Jiangsu Huachuang Cigna Pharmaceutical Technology Co., Ltd. The SW480 orthotopic xenograft tumor model was established by subcutaneous injection of SW480 cells (1×10^6) dispersed in 100 μL of PBS into the right front limb armpit of each mouse to a 3 mm depth. Tumor volume (V) was measured using vernier calipers and determined by measuring the length (L) and width (W), and calculated using Equations (5).

$$V = \frac{1}{2} \times L \times W^2$$

In vivo Antitumor Effect

When the tumor volumes reached 200–300 mm^3, the mice were randomly divided into four groups (n = 5). Mice were intraperitoneally injected with 100 μL of Cet-Iri-NPs or free CPT-11 at an equivalent CPT-11 dose of 15 mg/kg every two days. The control group was injected with an equal volume of PBS. For the laser treatment groups, the tumors of the mice were irradiated with an NIR laser (808 nm, 1.6 W/cm^2) for 5 min at 6 h post-injection. The body weight and tumor volume of each mouse were recorded every other day. The mice with tumor sizes exceeding 2000 m^3 were euthanized according to the animal protocol. After a 14-day injection period, mice were sacrificed by cervical dislocation. The major organs (heart, liver, spleen, lung, kidneys) and tumors were collected for semiquantitative biodistribution analysis. Paraffin embedding, sectioning, slide preparation, and hematoxylin and eosin staining (H&E) were carried out. All slices were observed under a fluorescence microscope. The tumor inhibition rate was calculated using Equations (6).

$$\text{Tumor inhibition rate}(\%) = \left(1 - \frac{\text{tumor weight}_{\text{test}}}{\text{tumor weight}_{\text{control}}}\right) \times 100$$

Results and Discussion

Characterization of Copolymer PPG-PEG

The polymer PPG was synthesized and conjugated with mPEG-NH_2 to obtain the PEGylated copolymer PPG-PEG (Figure 1). The chemical structure was investigated by 1H-NMR (Bruker-400) (Figure 2A) and FTIR (Thermo Scientific Nicolet iS5) (Figure 2B). The spectrum of ^{1}H-NMR (DMSO-d6) of the PPG-PEG illustrated the typical proton peaks of 6.41–8.10 ppm which were from the benzene ring of PPG chains, and 3.12–4.04 ppm which were contributed to the methylene unite of PEG side chains. As shown in Figure 2B, the absorption bands at 1592 cm^{-1} and 1506 cm^{-1} were related to the stretching bands of the quinoid and benzenoid rings in PPG main chain. After PPG reacted with mPEG-NH_2, these two characteristic absorption peaks were blue-shifted to 1558 cm^{-1} and 1466 cm^{-1}, respectively. Furthermore, the C-O-C stretching vibration of PPG was located at 1158 cm^{-1}, while the C-O-C stretching vibration of PPG-PEG moved to 1148 cm^{-1}. These may be due to the formation of a connection between the main chain and the PEG chain. Thus, we could presume that PPG-PEG was successfully synthesized via a condensation reaction between the carboxyl group of PPG and the amide group of mPEG-NH_2.

Physicochemical Characterization of Cet-Iri-NPs

The preparation scheme for cetuximab-modified and NIR-activated nanoparticles (abbreviated as Cet-Iri-NPs) was shown in Figure 3. First, CPT-loaded nanoparticles (abbreviated as Iri-NPs) were prepared with PPG-PEG, DSPE-PEG-Mal, lecithin, CPT-11, and ICG, using an ultrasonic emulsification method. Then the resulting green emulsion was gently stirred in the dark to evaporate organic solvent. Subsequently, Iri-NPs were further functionalized with the specific targeting ligand cetuximab through a reaction between maleimide groups on the surface of nanoparticles and the sulfhydryl groups of cetuximab, resulting in the expected green emulsion of Cet-Iri-NPs.

The morphology of Cet-Iri-NPs was evaluated using TEM and DLS. TEM confirmed that the Cet-Iri-NPs had a spherical shape with particle sizes ranging from 70 to 110 nm (Figure 4A). From the dynamic light scattering (DLS) measurements, the hydrodynamic size of Cet-Iri-NPs was estimated to be 99.88 ± 2.51 nm and PDI was 0.15 ± 0.03, which was in agreement with the particle size obtained from the TEM results (Figure 4B). The size distribution showed that the Cet-Iri-NPs were about 100 nm, indicating that they could improve drug delivery to tumors via an enhanced permeability and retention effect (EPR).[42–44] In addition, the surface potential of Cet-Iri-NPs was negatively charged at approximately −29.17 ± 3.09 mV

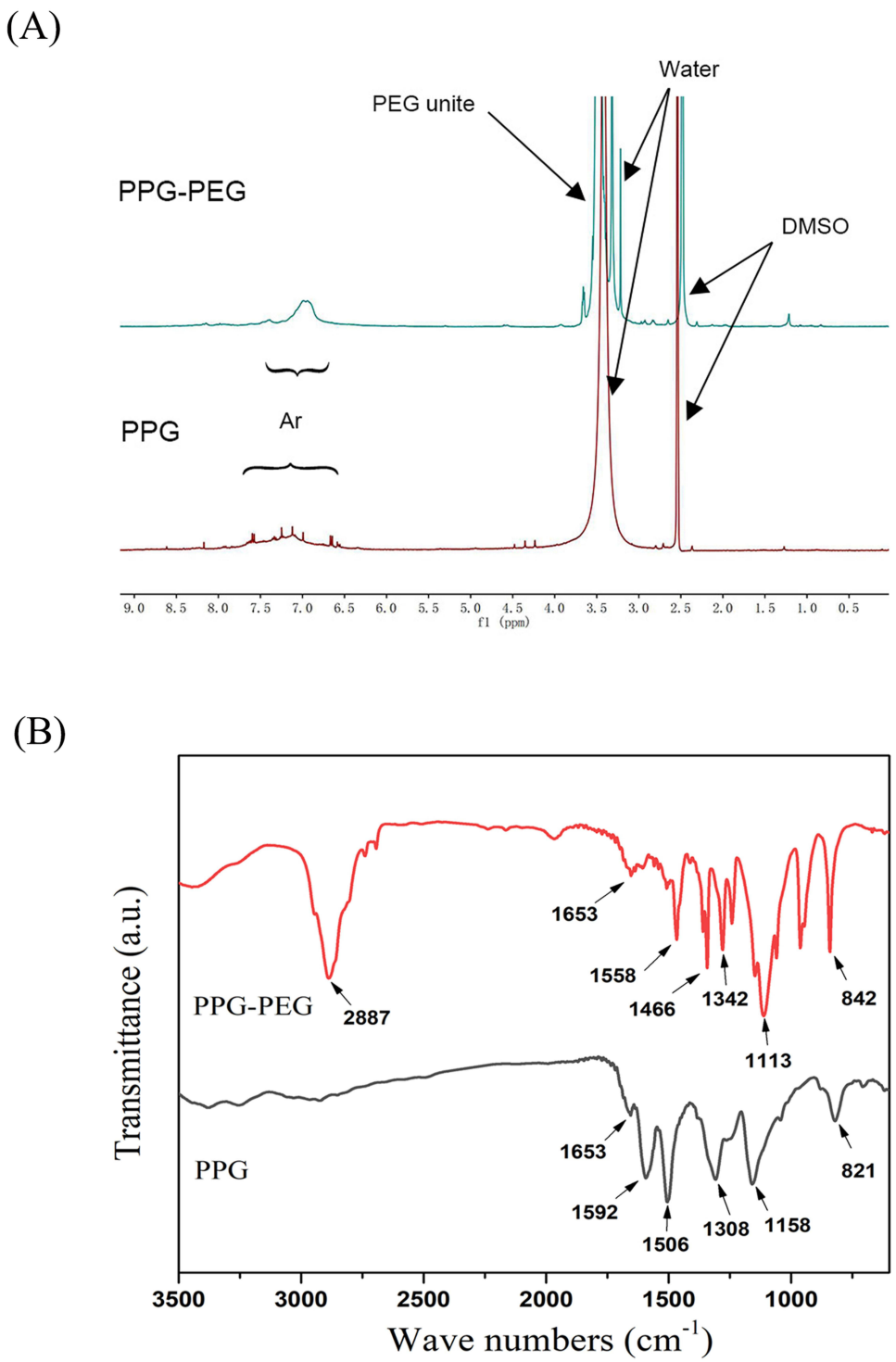

Figure 2 Characterization of synthesized polymers. (**A**) ^{1}H-NMR spectra and (**B**) FTIR spectrum of PPG and PPG-PEG.

(Figure 4C). More importantly, the loading efficiency (LE) of CPT-11 and ICG in Cet-Iri-NPs was measured to be ~21.55 wt % and ~27.14 wt% (encapsulation efficiency of CPT-11 and ICG was measured to be ~51.72% and ~65.13%), respectively. Thus, we conjectured that the small size, negative charge, and surface PEGylation may be beneficial for the EPR effect of Cet-Iri-NPs, as well as for the delayed macrophage clearance in the reticular endothelial system (RES), ensuring active tumor targeting with a long retention time in the bloodstream.[35,45] Based on the analysis of BCA research, about 41.70 wt% of

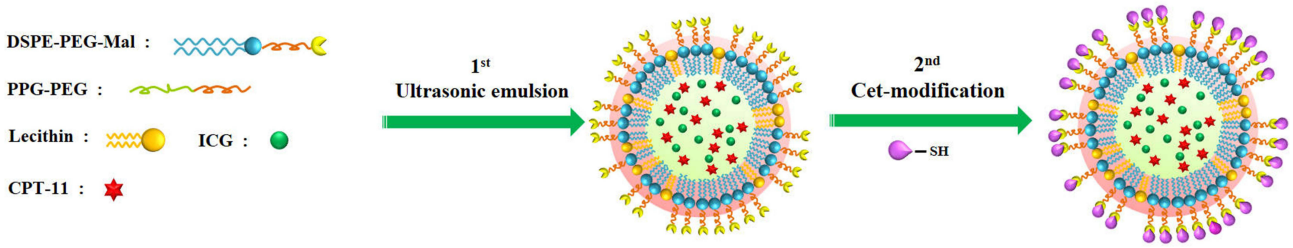

Figure 3 Scheme for the preparation of Cet-Iri-NPs.

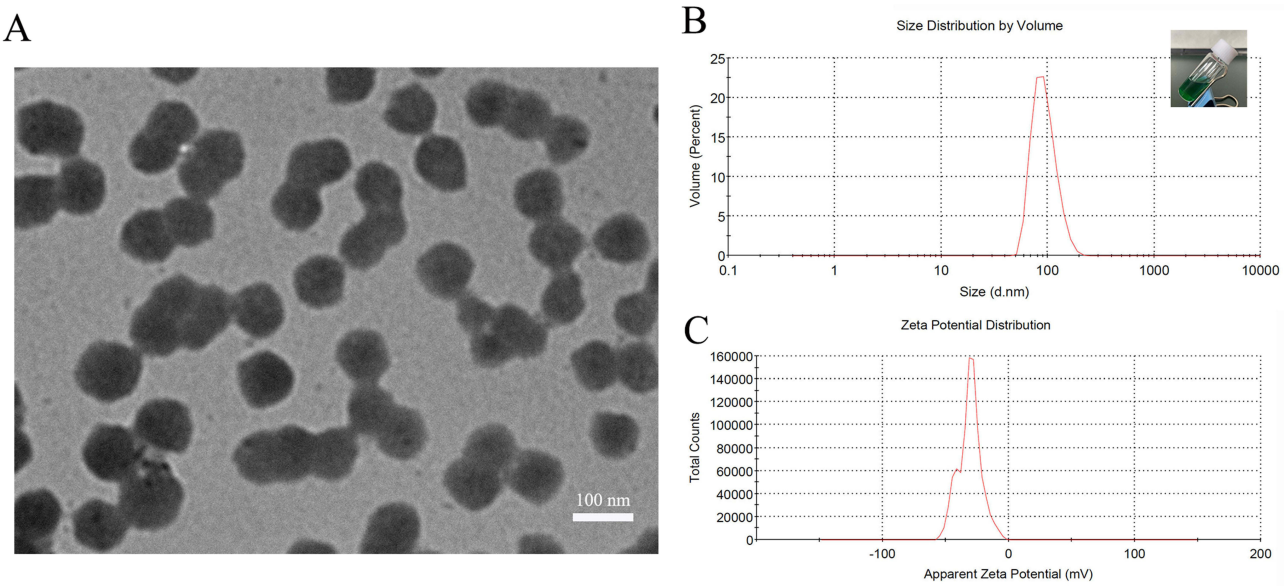

Figure 4 Characterization of Cet-Iri-NPs. (**A**) TEM image of Cet-Iri-NPs. (**B**) Size distribution and photographs of Cet-Iri-NPs dispersed in water. (**C**) Zeta potential of Cet-Iri-NPs measured by DLS.

cetuximab added to the reaction was conjugated on the surface of Cet-Iri-NPs, a percentage similar to those described in literature for other NPs,[46] supporting the adequacy of the conventional method for ligand conjugation.

Photothermal Effect and in vitro NIR-Triggered Drug Release

As ICG can effectively convert NIR light to heat, the photothermal effect of the ICG-loaded nanoparticles was evaluated by monitoring real-time temperatures after irradiation. At the same irradiation time, free ICG and Cet-Iri-NPs aqueous solution exhibited rapid responses to NIR light. However, PBS and Cet-Iri-NPs (without ICG-loaded) solutions exhibited a comparatively unapparent temperature variation (Figure 5A). After NIR irradiation (808 nm, 1.6 W/cm^2) for 5 min, the maximum temperature of free ICG and Cet-Iri-NPs aqueous solutions rose to 42.4°C and 45.1°C, respectively (Figure 5B), which would cause irreversible damage to tumor cells.[40,47] This may be due to the synergistic photothermal effect of the conjugated polymer PPG-PEG and ICG, as well as the interception of thermal radiation by nanoparticles, resulting in a higher photothermal conversion efficiency and better thermal retention of Cet-Iri-NPs after NIR irradiation.

Since the release of CPT-11 from Cet-Iri-NPs is preferable after endocytosis for maximum anticancer efficacy, the drug release process of Cet-Iri-NPs were investigated by the dialysis bag diffusion method at 37°C in pH 5.0 and 7.4 PBS to simulate the endosomal environment and the physiological conditions, respectively. The UV/vis absorption of CPT-11 outside the diffusion bag was detected. As shown in Figure 5C, a burst drug release behavior was observed in every group during the first 4 h. Subsequently, the release rates changed. Upon NIR irradiation, the cumulative release of CPT-11 from Cet-Iri-NPs in pH 5.0 and 7.4 PBS was about 59.29% and 49.99% during the first 24h, respectively. The release rates were more rapid than those laser-absent groups. Then, the release rates gradually slowed down. It is worth noting

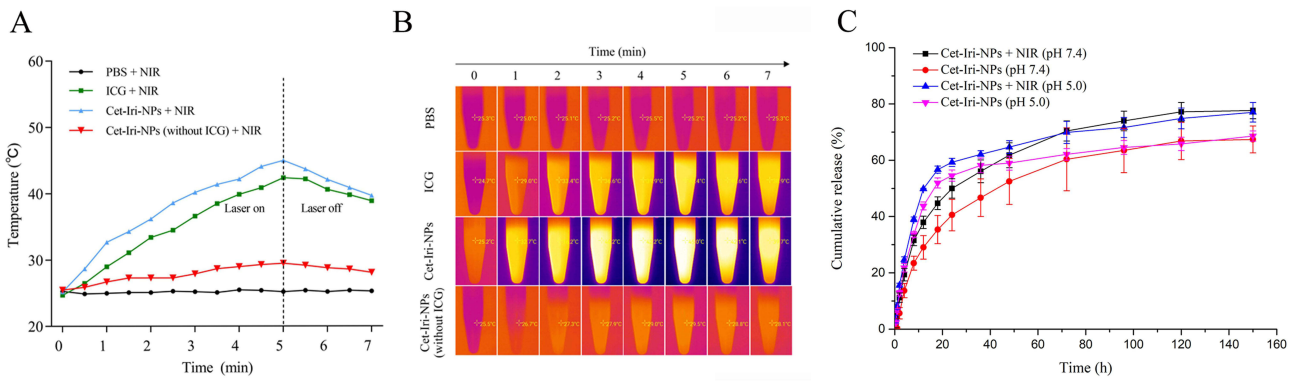

Figure 5 (**A**) Time-dependent temperature increase profiles and (**B**) infrared thermal imaging pictures of PBS, free ICG, Cet-Iri-NPs and Cet-Iri-NPs (without ICG) at different irradiation times (808 nm, 1.6 W/cm^2). (**C**) Cumulative release profiles of CPT-11 from Cet-Iri-NPs treated with NIR irradiation (808 nm, 1.6 W cm^{-2}, 5 min). Data were presented as mean ± S.D. (n = 3).

that the release rate in pH 5.0 was slightly faster than in 7.4 PBS during 80 h. But the final cumulative amount of CPT-11 was very close. After 150 h, the final cumulative amount of CPT-11 was about 77.06% at pH 5.0, and 77.66% at pH 7.4, respectively. These two similar release rates may be due to the fact that the hybrid NPs were sufficient swelling to allow full drug release. In contrast, the final cumulative amount of CPT-11 from Cet-Iri-NPs without NIR treatment was only about 67.41% at pH 5.0 and 68.62% at pH 7.4, respectively. These results implied that NIR laser irradiation could accelerate the dissociation release of CPT-11 from Cet-Iri-NPs no matter in pH 5.0 or 7.4 PBS. Such pH-responsive as well as NIR-triggered release properties may benefit drug release at tumor sites.[45,48] As a result, the efficacy of anti-cancer NPs could be significantly improved through high and sustained local drug concentrations in the tumor cells.

In vitro Cellular Uptake of Cet-Iri-NPs

In this study, CLSM was employed to assess the intracellular distribution of free ICG and Cet-Iri-NPs in EGFR-high-expressing SW480 cells[49,50] or in EGFR-negative-expressing MCF-7 cells.[51] As presented in Figure 6, blue fluorescence represented the cell nucleus and red fluorescence represented ICG. After 3 h incubation with free ICG, very weak red fluorescence was detected whether in SW480 or MCF-7 cells. In contrast, when SW480 cells were incubated with Cet-Iri-NPs, obvious red fluorescence signals of ICG were observed, indicating that a large number of nanoparticles had entered into the cytoplasm. Whereas the red fluorescence of Cet-Iri-NPs in the MCF-7 cells was still very weak. These results indicated that the surface modification of cetuximab could result in an efficient and specific association with EGFR high-expressing cells.[34] Meanwhile, the photothermal influence on cellular uptake was evaluated. After 5 min NIR irradiation and 3 h incubation, enhanced red fluorescence of Cet-Iri-NPs was detected in the cytoplasm of SW480 cells than that without NIR treatment, which is due to the fact that it was easier for the particles to be taken in by the cells and release ICG after incidence of the NIR laser. It was apparent that hyperthermia triggered by NIR irradiation quickly increased cell permeability and fluidity, thereby enhancing the drug accumulation inside cancer cells.[40,52] These results confirmed the intracellular process of Cet-Iri-NPs and their specific tumor-imaging capability for synergistic chemo-photothermal therapy.

Intracellular ROS Level of Cet-Iri-NPs

Non-fluorescent DCFH-DA was chosen as the reactive oxygen species (ROS) marker. In the presence of ROS, DCFH-DA would be hydrolyzed to DCF and yielded green fluorescent signals. As shown in Figure 7, weak green fluorescent signals were observed in the control groups (PBS and CPT-11) after 6 h of incubation. Meanwhile, the cells treated with ICG and Cet-Iri-NPs also presented a weak intracellular ROS signal. However, the ROS signal of ICG/NIR was slightly enhanced for the reason that ICG could generate ROS in cells under NIR irradiation.[40] Interestingly, upon NIR irradiation, the Cet-Iri-NPs groups showed higher ROS levels than ICG with NIR group. The higher amount of ROS generated by Cet-Iri-NPs under NIR irradiation was also considered to be vital for the implementation of synchronism in chemo-photothermal therapy.

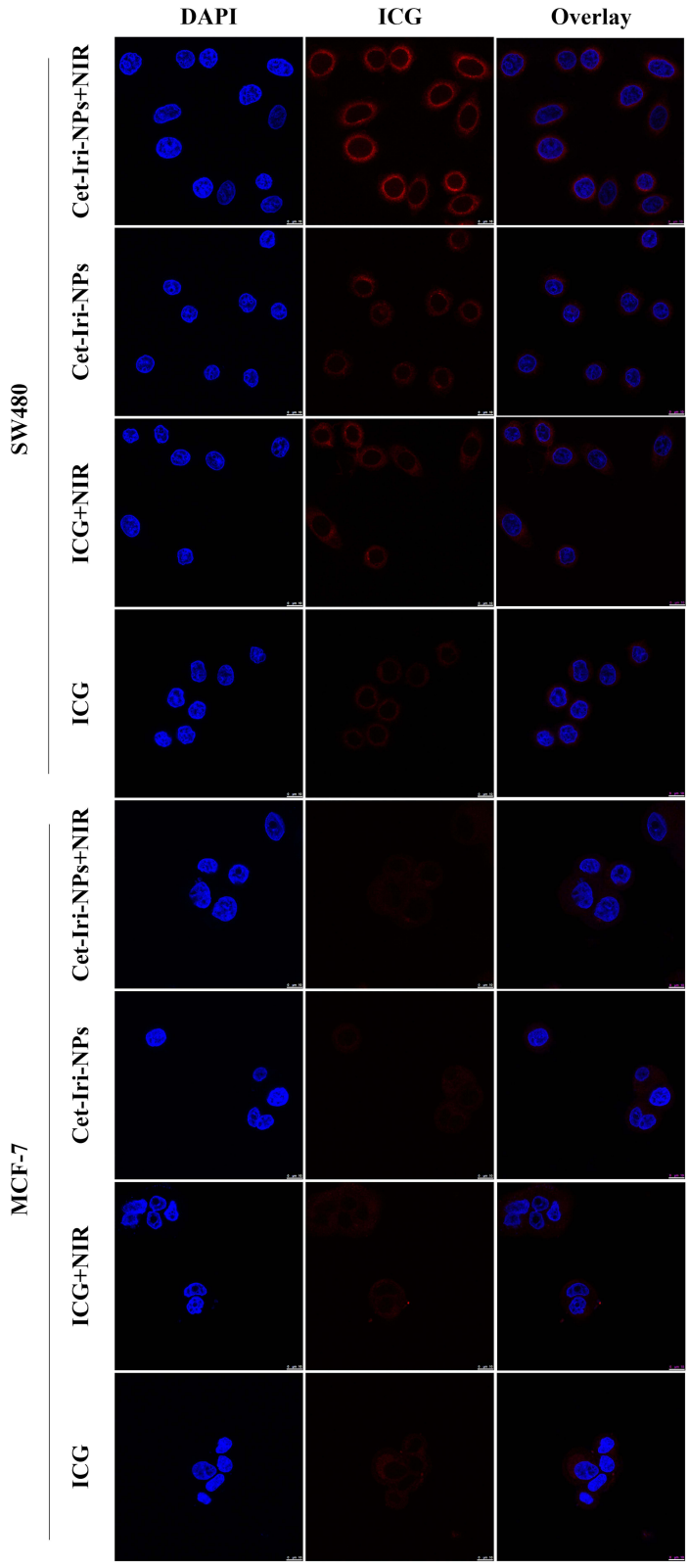

Figure 6 Confocal imaging of the cellular uptake of free ICG, Cet-Iri-NPs. Scale bars rare 10 μm.

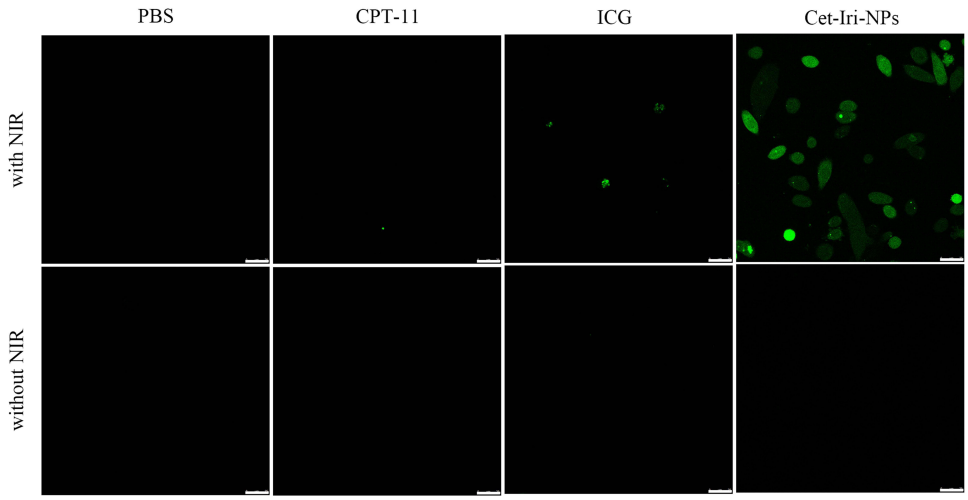

Figure 7 FL images of ROS generation in SW480 cells treated with PBS, CPT-11, ICG and Cet-Iri-NPs. (NIR: 808 nm, 5 min). Scale bars are 25μm.

In vitro Chemo-Photothermal Therapy of Cet-Iri-NPs

The CCK8 assay was used to evaluate the in vitro cytotoxicity and photothermal therapy of Cet-Iri-NPs in SW480 cells. Cells treated with free CPT-11 were chosen as controls. As shown in Figure 8A, the copolymer PPG-PEG represented high viability above 95% with a concentration range of 0.25–4 mg/mL, suggesting that PPG-PEG is nontoxic and has good biocompatibility. Furthermore, the tumor cells were treated with free CPT-11 and Cet-Iri-NPs at various drug concentrations. The results showed all samples inhibited tumor cell proliferation in a dose-dependent manner (Figure 8B). At low drug centration (1.25–5 μg/mL), the viability of cells treated with CPT-11 and Cet-Iri-NPs were very close. With the increase of drug content, CPT-11 induced more cell death than Cet-Iri-NPs did. At the CPT-11 concentration of 80 μg/mL, the cell viability of free CPT-11 and Cet-Iri-NPs was about 46% and 78%, respectively. However, under laser irradiation, the inhibition efficiency of Cet-Iri-NPs enhanced with the increase of drug concentration. Cet-Iri-NPs with NIR induced up to about 96% cell death. The IC_{50} of Cet-Iri-NPs with NIR irradiation against SW480 cells was 9.00 ± 1.05 μg/mL, which was obviously lower than 72.01 ± 1.29 μg/mL of CPT-11. Overall, the NIR laser triggered faster drug release and the synchronous photothermal effect of Cet-Iri-NPs efficiently promoted the inhibition rate of tumor cells.

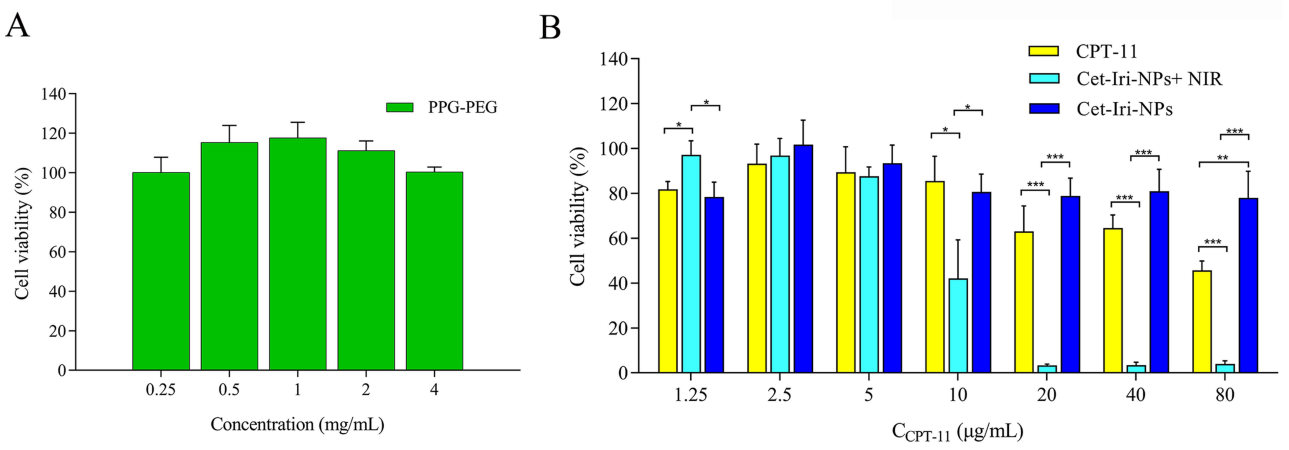

Figure 8 In vitro cytotoxicity and biocompatibility. (**A**) Cell viability of SW480 cells treated with PPG-PEG. (**B**) Cell viability of SW480 cells treated with free CPT-11, Cet-Iri-NPs with or without 5 min NIR irradiation at various CPT-11 concentrations. Data were presented as mean ± SD (n = 3). *P < 0.05, **P < 0.01, and ***P < 0.001.

Cell Apoptosis of Cet-Iri-NPs

To demonstrate the apoptosis-inducing capability of Cet-Iri-NPs, the Annexin V-FITC/PI apoptosis detection was performed to compare with laser, free ICG, ICG/NIR, free CPT-11, and free CPT-11/NIR groups. As shown in Figure 9, very few apoptotic cells were identified in the control group, whereas the free ICG, CPT-11, and Cet-Iri-NPs groups showed more cell apoptosis. Moreover, there was no significant difference between the free ICG and CPT-11 whether irradiated with an NIR laser. However, the combination treatment group of Cet-Iri-NPs irradiated by NIR laser exhibited the highest total cell apoptosis rate of 35.82%, which confirmed that the remarkable enhancement of apoptosis-inducing activity resulted from chemo-photothermal synergistic effect.[17,34]

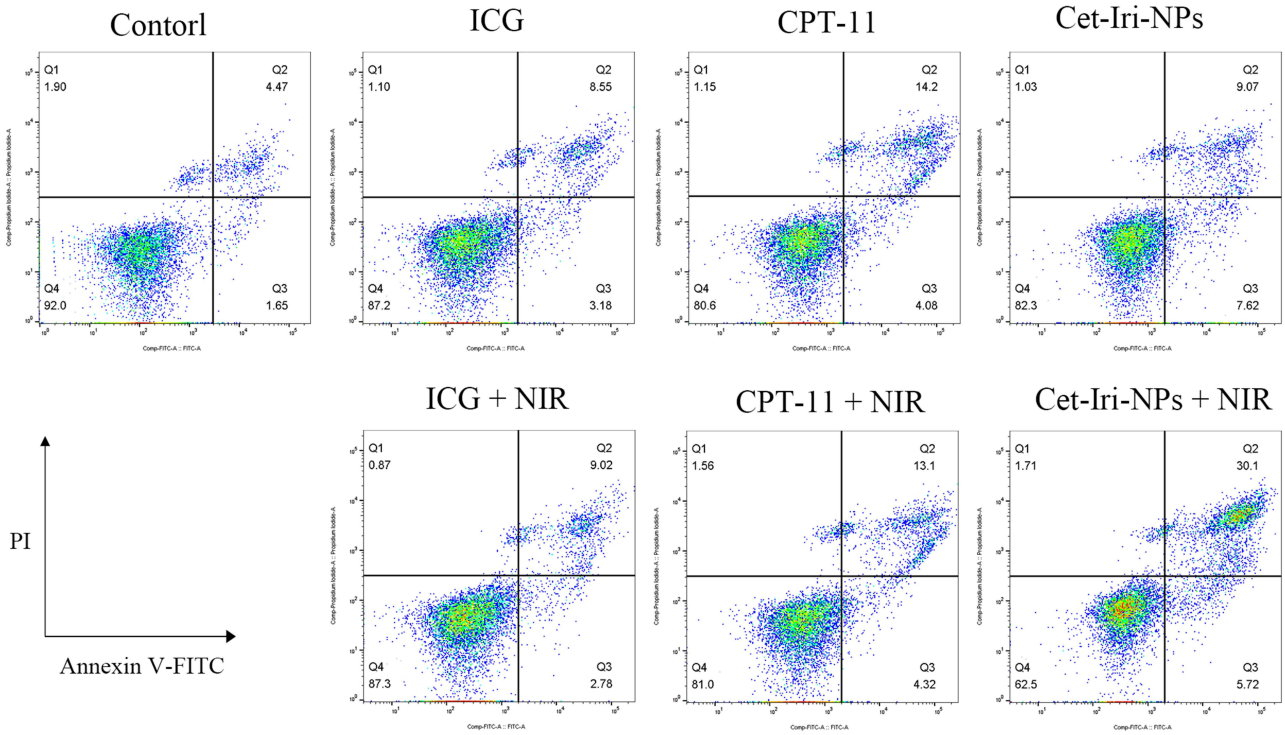

Figure 9 Flow cytometry analysis of sw480 cells after 24 h incubation with free CPT-11, free ICG, Cet-Iri-NPs (with or without NIR laser irradiation).

In vivo Chemo-Photothermal Therapy and Biosafety

The antitumor efficacy of Cet-Iri-NPs (with or without NIR irradiation) compared with CPT-11 was further evaluated in SW480 xenograft models at a 15 mg/kg paclitaxel equivalent dose in vivo. During the treatment of tumor-bearing mice, the tumor volume and body weight of the mice were measured every other day. There was no significant change in body weight during the treatment period, indicating that the treatments at the tested doses were well tolerated (Figure 10A). As shown in Figure 10B, SW480 tumors treated with PBS grew rapidly. Free CPT-11 and Cet-Iri-NPs could effectively inhibit tumor growth. Upon NIR irradiation, the tumor-inhibition effect of Cet-Iri-NPs was slightly improved. At 2 weeks after treatment, mean tumor volume treated with CPT-11 was ~39.57 mm^3, Cet-Iri-NPs of ~63.76 mm^3, Cet-Iri-NPs with NIR of ~29.12 mm^3 and PBS as control of ~628.44 mm^3 (Figure 10C and D).

Hematoxylin and eosin (H&E) staining was used to stain SW480 tumor tissues at 2 weeks post-treatment. As shown in Figure 11, tumor tissues from the PBS control group had relatively intact nuclei. Compared with free CPT-11 and Cet-Iri-NPs, Cet-Iri-NPs with NIR laser irradiation exhibited more pronounced necrosis and tumor cells with more irregular shapes and mitoses. It also revealed the synergistic chemotherapy and PTT effects. At the same time, the Cet-Iri-NPs' toxicity to major organs was further investigated by H&E staining. There were no obvious pathological abnormalities in the Cet-Iri-NPs and Cet-Iri-NPs plus NIR therapy groups, which means that they had no apparent abnormal damage on normal tissues, further proving the

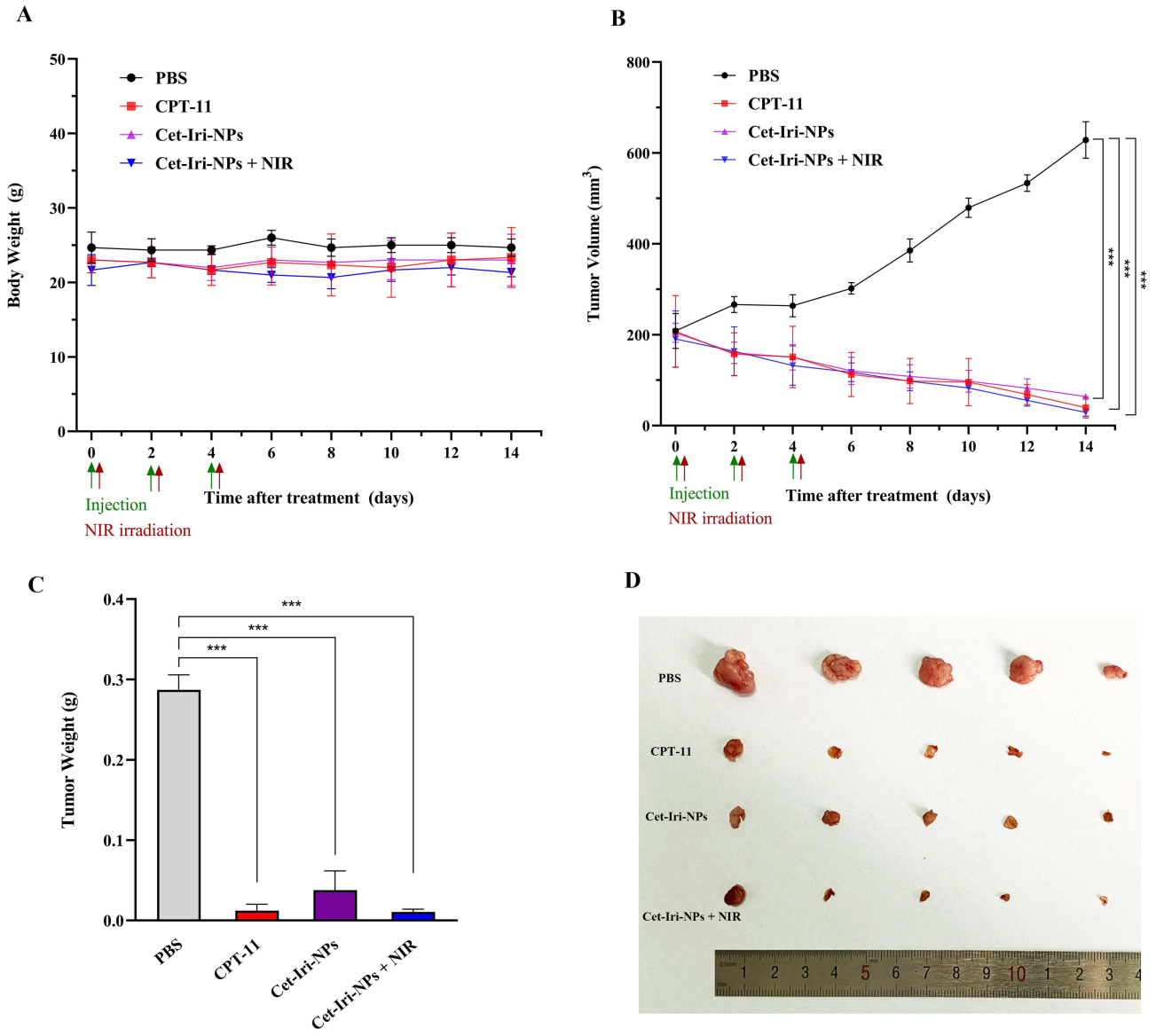

Figure 10 Antitumor activity of different treatments on SW480 xenograft nude mice. (**A**) Body weight change. (**B**) Tumor growth. (**C**) Tumor weight. (**D**) Tumor size map at the experimental end-point.*P < 0.05, **P < 0.01, and ***P < 0.001.

biocompatibility of the constructed NPs in the tested dosage range. These aforementioned data all confirmed that Cet-Iri-NPs plus NIR irradiation had great potential in improving the anti-cancer therapeutic efficacy and reducing the corresponding adverse effects.

Conclusion

In this study, a new class of tumor-targeted and NIR-activated nanoparticles (Cet-Iri-NPs) was successfully constructed, which was effectively overcame the lack of selectivity of CPT and ICG while demonstrating strong growth inhibitory effects on CRC cells. The designed Cet-Iri-NPs exhibited suitable size distribution, surface charge, and pH/NIR dual-response drug release properties. Moreover, Cet-Iri-NPs with NIR laser irradiation exhibited remarkable cellular uptake, high ROS levels, and superior cytotoxic activity compared to the control groups in EGFR high-expressing SW480 cells. In addition, in vivo imaging and antitumor activity further certificated the outstanding targeting ability and chemo-photothermal combined antitumor activity of Cet-Iri-NPs under NIR laser irradiation. Therefore, this work presents that Cet-Iri-NPs could be used as a versatile drug delivery nanoplatform for human CRC therapy.

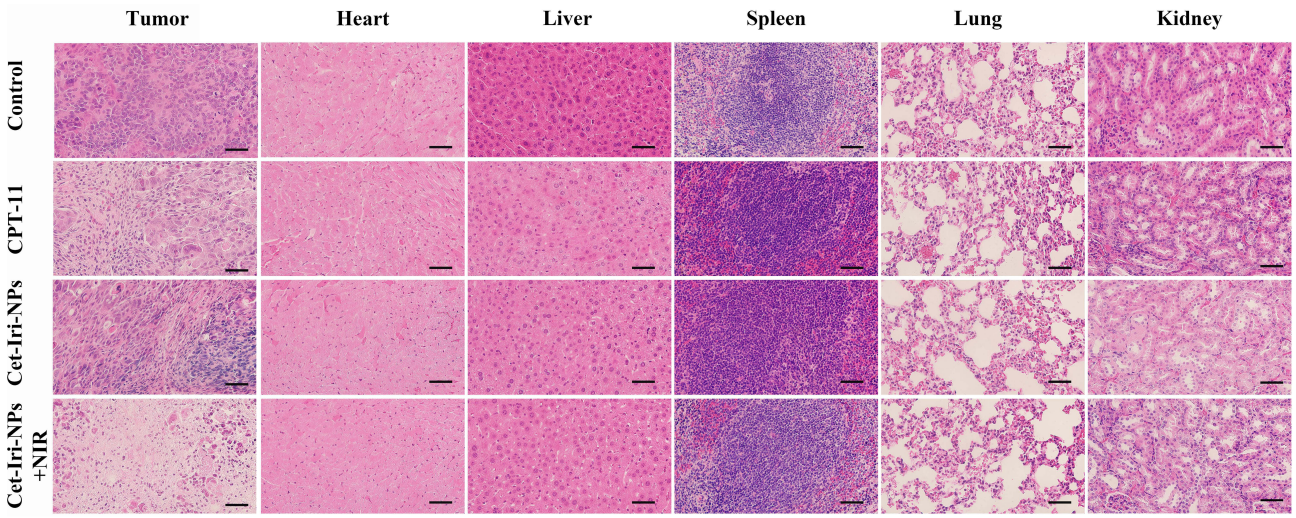

Figure 11 H&E stained histological images from normal (including heart, liver, spleen, lung, and kidney) and tumor tissues of SW480 xenograft nude mice.

Acknowledgment

This work was supported by the Natural Science Research Project of the Anhui Educational Committee (2023AH040249) and the Anhui Provincial Natural Science Foundation (2108085QH370).

Disclosure

The authors report no conflicts of interest in this work.

References

1. Sung H, Ferlay J, Siegel RL, et al. Global Cancer Statistics 2020: GLOBOCAN Estimates of Incidence and Mortality Worldwide for 36 Cancers in 185 Countries. *CA Cancer J Clin*. 2021;71(3):209–249. doi:10.3322/caac.21660
2. Zhong X, He X, Wang Y, et al. Warburg effect in colorectal cancer: the emerging roles in tumor microenvironment and therapeutic implications. *J Hematol Oncol*. 2022;15(1):160. doi:10.1186/s13045-022-01358-5
3. Biller LH, Schrag D. Diagnosis and treatment of metastatic colorectal cancer: a review. *JAMA*. 2021;325(7):669–685. doi:10.1001/jama.2021.0106
4. Bailly C. Irinotecan: 25 years of cancer treatment. *Pharmacol Res*. 2019;148:104398. doi:10.1016/j.phrs.2019.104398
5. Zhang Y, Yue X, Yang S, et al. Long circulation and tumor-targeting biomimetic nanoparticles for efficient chemo/photothermal synergistic therapy. *J Mater Chem B*. 2022;10(26):5035–5044. doi:10.1039/d2tb00748g
6. Li Y, Su Y, Pan H, et al. Nanodiamond-based multifunctional platform for oral chemo-photothermal combinational therapy of orthotopic colon cancer. *Pharmacol Res*. 2022;176:106080. doi:10.1016/j.phrs.2022.106080
7. Lu Y, Chen L, Wu ZX, et al. Self-driven bioactive hybrids co-deliver doxorubicin and indocyanine green nanoparticles for chemo/photothermal therapy of breast cancer. *Biomed Pharmacother*. 2023;169:115846 doi:10.1016/j.biopha.2023.115846.
8. Farokhia M, Mottaghitalabb F, Saebc MR, Thomasd S. Functionalized theranostic nanocarriers with bio-inspired polydopamine for tumor imaging and chemo-photothermal therapy. *J Control Release*. 2019;309:203–219. doi:10.1016/j.jconrel.2019.07.036
9. Deng K, Tian H, Zhang T, et al. Chemo-photothermal nanoplatform with diselenide as the key for ferroptosis in colorectal cancer. *J Control Release*. 2024;366:684–693. doi:10.1016/j.jconrel.2024.01.024
10. Liu Q, Song P, Zhang W, et al. Acid-sensitive nanoparticles based on molybdenum disulfide for photothermal-chemo therapy. *ACS Biomater Sci Eng*. 2022;8(4):1706–1716. doi:10.1021/acsbiomaterials.1c01390
11. Yin M, Yang M, Yan D, et al. Surface charge switchable and size transformable thermosensitive nanocomposites for chemo-photothermal eradication of bacterial biofilms in vitro and in vivo. *ACS Appl Mater Inter*. 2022;14(7):8847–8864. doi:10.1021/acsami.1c24229
12. Zhang XY, Lai YK, Zhang L, et al. Chitosan-modified molybdenum selenide mediated efficient killing of *Helicobacter pylori* and treatment of gastric cancer. *Int J Biol Macromol*. 2024;275:133599. doi:10.1016/j.ijbiomac.2024.133599
13. Xu PY, Zheng X, Kankala RK et al. Advances in indocyanine green-based codelivery nanoplatforms for combinatorial therapy. *ACS Biomater Sci Eng*. 2021;7(3):939–962. doi:10.1021/acsbiomaterials.0c01644
14. Porcu EP, Salis A, Gavini E et al. Indocyanine green delivery systems for tumour detection and treatments. *Biotechnol Adv*. 2016;34(5):768–789. doi:10.1016/j.biotechadv.2016.04.001
15. Li Z, Chen Y, Yang Y, et al. Recent advances in nanomaterials-based chemo-photothermal combination therapy for improving cancer treatment. *Front Bioeng Biotech*. 2019;7:293. doi:10.3389/fbioe.2019.00293
16. Liu C, Ruan C, Shi R et al. A near infrared-modulated thermosensitive hydrogel for stabilization of indocyanine green and combinatorial anticancer phototherapy. *Biomater Sci*. 2019;7(4):1705–1715. doi:10.1039/c8bm01541d

17. Tang L, Xiao Q, Yin Y, et al. An enzyme-responsive and NIR-triggered lipid-polymer hybrid nanoplatform for synergistic photothermal/chemo cancer therapy. *Biomater Sci*. 2022;10(9):2370–2383. doi:10.1039/d2bm00216g
18. Patel V, Rajani C, Tambe V, et al. Nanomaterials assisted chemo-photothermal therapy for combating cancer drug resistance. *J Drug Delivery Sci Technol*. 2022;70:103164. doi:10.1016/j.jddst.2022.103164
19. Hossen S, Hossain MK, Basher MK et al. Smart nanocarrier-based drug delivery systems for cancer therapy and toxicity studies: a review. *J Adv Res*. 2019;15:1–18. doi:10.1016/j.jare.2018.06.005
20. Hong HD, Zou QL, Liu YM et al. Supramolecular nanodrugs based on covalent assembly of therapeutic peptides toward synergistic anticancer therapy. *Chem Med Chem*. 2021;16(15):2381–2385. doi:10.1002/cmdc.202100236
21. Fatima H, Naz MY, Shukrullah S et al. A review of multifunction smart nanoparticle based drug delivery systems. *Curr Pharm Des*. 2022;28 (36):2965–2983. doi:10.2174/1381612828666220422085702
22. Kolate A, Baradia D, Patil S et al. PEG-A versatile conjugating ligand for drugs and drug delivery systems. *J Control Release*. 2014;192:67–81. doi:10.1016/j.jconrel.2014.06.046
23. Nezhad-Mokhtari P, Ghorbani M, Mahmoodzadeh F. Smart co-delivery of 6-mercaptopurine and methotrexate using disulphide-based PEGylated-nanogels for effective treatment of breast cancer. *New J Chem*. 2019;43(30):12159–12167. doi:10.1039/c9nj02470k
24. Chen YY, Guo MF, Qu D et al. Furin-responsive triterpenine-based liposomal complex enhances anticervical cancer therapy through size modulation. *Drug Delivery*. 2020;27(1):1608–1624. doi:10.1080/10717544.2020.1827086
25. Chen YY, Wang SZ, Hu QY et al. Self-emulsifying system co-loaded with paclitaxel and coix seed oil deeply penetrated to enhance efficacy in cervical cancer. *Curr Drug Deliv*. 2023;20(7):919–926. doi:10.2174/1567201819666220628094239
26. Yoo J, Park C, Yi G et al. Active targeting strategies using biological ligands for nanoparticle drug delivery systems. *Cancers*. 2019;11(5):640. doi:10.3390/cancers11050640
27. Zhao Z, Ukidve A, Kim J et al. Targeting strategies for tissue-specific drug delivery. *Cell*. 2020;181(1):151–167. doi:10.1016/j.cell.2020.02.001
28. Chen Y, Zhang Z, Qian Z et al. Sequentially Released Liposomes Enhance Anti-Liver Cancer Efficacy of Tetrandrine and Celastrol-Loaded Coix Seed Oil. *Int J Nanomed*. 2024;19:727–742. doi:10.2147/ijn.S446895
29. Saoudi González N, Ros J, Baraibar I, et al. Cetuximab as a key partner in personalized targeted therapy for metastatic colorectal cancer. *Cancers*. 2024;16(2):412. doi:10.3390/cancers16020412
30. Sakai D, Taniguchi H, Sugimoto N, et al. Randomised Phase II study of panitumumab plus irinotecan versus cetuximab plus irinotecan in patients with KRAS wild-type metastatic colorectal cancer refractory to fluoropyrimidine, irinotecan and oxaliplatin (WJOG 6510G). *Eur J Cancer*. 2020;135:11–21. doi:10.1016/j.ejca.2020.04.014
31. Ge XJ, Jiang JY, Wang M, et al. Cetuximab enhances the efficiency of irinotecan through simultaneously inhibiting the MAPK signaling and ABCG2 in colorectal cancer cells. *Pathol Res Pract*. 2020;216(2):152798. doi:10.1016/j.prp.2019.152798
32. Chang MH, Pai CL, Chen YC et al. Enhanced Antitumor Effects of Epidermal Growth Factor Receptor Targetable Cetuximab-Conjugated Polymeric Micelles for Photodynamic Therapy. *Nanomaterials*. 2018;8(2). doi:10.3390/nano8020121
33. Sabra R, Billa N, Roberts CJ. Cetuximab-conjugated chitosan-pectinate (modified) composite nanoparticles for targeting colon cancer. *Int J Pharm*. 2019;572:118775. doi:10.1016/j.ijpharm.2019.118775
34. Wang Y, Zhang XM, Sun Y et al. Cetuximab-decorated and NIR-activated nanoparticles based on platinum(iv)-prodrug: preparation, characterization and in-vitro anticancer activity in epidermoid carcinoma cells. *Iran J Pharm Res*. 2021;20(1):371–383. doi:10.22037/ijpr.2020.113439.14303
35. Fang F, Zhang X, Tang J et al. EGFR-targeted hybrid lipid nanoparticles for chemo-photothermal therapy against colorectal cancer cells. *Chem Phys Lipids*. 2023;251:105280. doi:10.1016/j.chemphyslip.2023.105280
36. Liu C, Guo X, Ruan C, et al. An injectable thermosensitive photothermal-network hydrogel for near-infrared-triggered drug delivery and synergistic photothermal-chemotherapy. *Acta Biomater*. 2019;96:281–294. doi:10.1016/j.actbio.2019.07.024
37. Sun Y, Shi T, Zhou L et al. Folate-decorated and NIR-activated nanoparticles based on platinum(IV) prodrugs for targeted therapy of ovarian cancer. *J Microencapsul*. 2017;34(7):675–686. doi:10.1080/02652048.2017.1393114
38. Liao WS, Ho Y, Lin YW, et al. Targeting EGFR of triple-negative breast cancer enhances the therapeutic efficacy of paclitaxel- and cetuximab-conjugated nanodiamond nanocomposite. *Acta Biomater*. 2019;86:395–405. doi:10.1016/j.actbio.2019.01.025
39. Wang J, Guo HM. Astragaloside IV ameliorates high glucose-induced HK-2 cell apoptosis and oxidative stress by regulating the Nrf2/ARE signaling pathway. *Exp Ther Med*. 2019;17(6):4409–4416. doi:10.3892/etm.2019.7495
40. Chen Y, Li H, Deng Y et al. Near-infrared light triggered drug delivery system for higher efficacy of combined chemo-photothermal treatment. *Acta Biomater*. 2017;51:374–392. doi:10.1016/j.actbio.2016.12.004
41. Li L, Lu B, Fan Q, et al. Synthesis and pH-responsive self-assembly behavior of a fluorescent amphiphilic triblock copolymer mPEG-b-PCL-b-PDMAEMA-g-PC for the controlled intracellular delivery of doxorubicin. *RSC Adv*. 2016;6(32):27102–27112. doi:10.1039/c6ra01504b
42. Hatakeyama H, Akita H, Harashima H. A multifunctional envelope type nano device (MEND) for gene delivery to tumours based on the EPR effect: a strategy for overcoming the PEG dilemma. *Adv Drug Deliv Rev*. 2011;63(3):152–160. doi:10.1016/j.addr.2010.09.001
43. Maruyama K. Intracellular targeting delivery of liposomal drugs to solid tumors based on EPR effects. *Adv Drug Deliv Rev*. 2011;63(3):161–169. doi:10.1016/j.addr.2010.09.003
44. Guo F, Yu M, Wang J et al. Smart IR780 theranostic nanocarrier for tumor-specific therapy: hyperthermia-mediated bubble-generating and folate-targeted liposomes. *ACS Appl Mater Inter*. 2015;7(37):20556–20567. doi:10.1021/acsami.5b06552
45. Li Y, Liu G, Ma J, et al. Chemotherapeutic drug-photothermal agent co-self-assembling nanoparticles for near-infrared fluorescence and photoacoustic dual-modal imaging-guided chemo-photothermal synergistic therapy. *J Control Release*. 2017;258:95–107. doi:10.1016/j.jconrel.2017.05.011
46. PG ME, Bell O, Agirre M, et al. Selective antitumoral effect of sorafenib loaded PLGA nanoparticles conjugated with cetuximab on undifferentiated anaplastic thyroid carcinoma cells. *Nanomed Nanotech*. 2015;6(3):1000281. doi:10.4172/2157-7439.100028110.4172/21577439.1000281
47. Lim YT, Noh YW, Han JH et al. Biocompatible polymer-nanoparticle-based bimodal imaging contrast agents for the labeling and tracking of dendritic cells. *Small*. 2008;4(10):1640–1645. doi:10.1002/smll.200800582
48. Li M, Zhang X, Zhou Y, et al. Near Infrared-Activatable Biomimetic Nanoplatform for Tumor-Specific Drug Release, Penetration and Chemo-Photothermal Synergistic Therapy of Orthotopic Glioblastoma. *Int J Nanomed*. 2024;19:6999–7014. doi:10.2147/ijn.S466268

49. Lan Z, Xin-Shan D, Guang-Peng M, et al. Design, synthesis and biological evaluation of a novel series of indole-3-carboxamide derivatives for cancer treatment as EGFR inhibitors. *Lett Drug Des Discov*. 2018;15:70–83. doi:10.2174/1570180814666170929093258
50. AWI L, Shigeta K, Hayashida T, et al. Expression of epidermal growth factor receptor detected by cetuximab indicates its efficacy to inhibit in vitro and in vivo proliferation of colorectal cancer cells. *PLoS One*. 2013;8(6):e66302. doi:10.1371/journal.pone.0066302
51. Chen Y, Liu G, Guo L et al. Enhancement of tumor uptake and therapeutic efficacy of EGFR-targeted antibody cetuximab and antibody-drug conjugates by cholesterol sequestration. *Int, J, Cancer*. 2015;136(1):182–194. doi:10.1002/ijc.28950
52. Zhang H, Sun Y, Huang R et al. pH-sensitive prodrug conjugated polydopamine for NIR-triggered synergistic chemo-photothermal therapy. *Eur J Pharm Biopharm*. 2018;128:260–271. doi:10.1016/j.ejpb.2018.05.013